

Enhanced metal-support interaction between Pd and hierarchical Nb₂O₅ via oxygen defects induction to promote CO oxidative coupling to dimethyl oxalate

Hongzi Tan ^{a#}, Yu-Ping Xu ^{b, d#}, Siteng Rong ^a, Rongrong Zhao ^a, Hongyou Cui ^{*a},
Zhe-Ning Chen ^{*b}, Zhong-Ning Xu ^b, Ning-Ning Zhang ^c and Guo-Cong Guo ^{*b}

^a School of Chemistry & Chemical Engineering, Shandong University of Technology, Zibo, Shandong 255049, P. R. China.

^b State Key Laboratory of Structural Chemistry, Fujian Institute of Research on the Structure of Matter, Chinese Academy of Sciences, Fuzhou, Fujian 350002, P. R. China.

^c School of Chemistry and Chemical Engineering, Liaocheng University, Liaocheng, Shandong 252000, P. R. China.

^d University of Chinese Academy of Sciences, Beijing 100049, P.R. China.

These authors contribute equally.

*To whom correspondence should be addressed: E-mail: cuihy@sdut.edu.cn; znchen@fjirsm.ac.cn; gcguo@fjirsm.ac.cn

Experimental Section

Catalyst Preparation

Chemical Materials. Pd(OAc)₂ (AR; Kunming Institute of Precious Metals); Nb(HC₂O₄)₅·xH₂O (AR; Aladdin Chemical Reagent Co., Ltd.); commercial Nb₂O₅ (AR; Aladdin Chemical Reagent Co., Ltd.); (NH₄)₂CO₃ (AR; Aladdin Chemical Reagent Co., Ltd.); acetone (AR; Sino-Pharm Chemical Regent Co., Ltd., China); ethanol (AR; Sino-Pharm Chemical Regent Co., Ltd., China); deionized water (18 MΩ·cm) were used throughout the experiments. All chemical materials in the experiment were used as received without further purification.

Preparation of hierarchical Nb₂O₅ (H-Nb₂O₅) microspheres. Firstly, 1.614 g of Nb(HC₂O₄)₅·xH₂O was dispersed in 50 mL of water containing 1.44 g of (NH₄)₂CO₃ under vigorous stirring for 10 min at room temperature. Secondly, the slurry was transferred into a 100 mL Teflon container, maintained at 200 °C for 12 h, and then cooled naturally. Thirdly, the synthesized solid product was centrifuged and washed with distilled water and ethanol for three times. Finally, the as-prepared sample was finally dried and calcined in air atmosphere at 550 °C for 5 h.

Preparation of Pd/H-Nb₂O₅ catalysts. A series of H-Nb₂O₅ supported Pd catalysts with designed Pd contents of 0.1 wt.%, 0.3 wt.%, 0.5 wt.%, 1.0 wt.% and 2.0 wt. % respectively were prepared via wet impregnation and reduction method by controlling the amount of the Pd(OAc)₂ precursor. The H-Nb₂O₅ support was impregnated with an acetone solution of Pd(OAc)₂ under vigorous stirring and then the suspension was evaporated under vacuum at 60 °C to remove the solvent and followed by calcination at 450 °C in air atmosphere for 2 h. Finally, the sample was reduced at 400 °C in H₂ atmosphere for 2 h, which was denoted as 0.1%-Pd/H-Nb₂O₅ (Cat-1), 0.3%-Pd/H-Nb₂O₅ (Cat-2), 0.5%-Pd/H-Nb₂O₅ (Cat-3), 1.0%-Pd/H-Nb₂O₅ (Cat-4) or 2.0%-Pd/H-Nb₂O₅ (Cat-5), according to the Pd content.

Preparation of Pd/C-Nb₂O₅ catalysts. The preparation procedure of Pd/C-Nb₂O₅ catalyst with 1.0 wt.% designed Pd content was nearly identical to that of Pd/H-Nb₂O₅ catalyst except replacing H-Nb₂O₅ with commercial Nb₂O₅ (C-Nb₂O₅).

Catalyst Characterization

Inductively coupled plasma (ICP) spectroscopy was recorded with an Ultima 2

plasma emission spectrometer from Jobin Yvon.

The morphologies of the samples were observed by JEOLJSM-6700F scanning electron microscopy (SEM).

X-ray photoelectron spectroscopy (XPS) were measured by an ESCALAB 250 Xi spectrometer equipped with an Al anode (K_{α} =1486.6 eV). All samples were pressed into a wafer prior to analysis.

Powder X-ray diffractions (PXRD) of all samples were collected by a Rigaku MiniFlex II diffractometer with a Cu K_{α} X-ray source (λ =1.5406 Å). The silicon wafer was used for testing and the test of 2θ was in the range of 5~85°.

Fourier translation infrared (FT-IR) spectroscopy was measured using a Perkin-Elmer Spectrum One FT-IR spectrophotometer in the range of 4000-400 cm^{-1} . The samples were finely grounded, dispersed in KBr and pelletized.

Brunauer–Emmett–Teller (BET) surface areas were calculated from the N_2 adsorption-desorption isotherms that were acquired on an ASAP 2020 instrument (Micromeritics) at 77 K. Prior to measurement, the samples were subject to evacuation at 200°C overnight.

Transmission electron microscopy (TEM) and high-resolution TEM (HRTEM) analysis were performed on a Tecnai G2 F20 field-emission transmission electron microscope operating at an acceleration voltage of 200 kV. The samples were prepared by dropping an ethanol dispersion of samples onto carbon-coated copper grids with a pipettor, and the solvent was allowed to evaporate at room temperature.

H_2 Temperature programmed reduction (H_2 -TPR) was carried out using an Altamira AMI-300 instrument equipped with a thermal conductivity detector. Prior to conducting the H_2 -TPR experiment, 100 mg of sample placed in a quartz U-tube was first heated to 400 °C for 1 h under a flow of argon (30 $\text{mL}\cdot\text{min}^{-1}$). After cooling to room temperature, the sample was exposed to 10% H_2 -Ar mixture (30 $\text{mL}\cdot\text{min}^{-1}$) and then heated to 500 °C at a rate of 10 °C $\cdot\text{min}^{-1}$.

NH_3 temperature programmed desorption (NH_3 -TPD) was carried out using an Altamira AMI-300 instrument equipped with a thermal conductivity detector. 100 mg sample was treated in a flow of He at 600 °C for 1.0 h to remove the adsorbed impurities. After cooling to 30 °C in a flow of He, the sample was exposed to 10%

NH₃/He mixture for 2.0 h (30 mL·min⁻¹), followed by purging with He for 30 min, and then heated to 800 °C by ramping at 10 °C·min⁻¹ under a flow of He.

in situ pyridine-adsorbed FTIR spectra were used to discriminate acid type of samples on a Thermo fisher Nicolet IS10. Wafers of compressed catalysts samples were mounted in the FTIR cell and degassed in vacuum of 10⁻⁷ Pa at 573 K for 2 h. The samples were saturated with pyridine vapor at 303 K for 10 min to reach an equilibration, and then evacuated at 373 K to remove the excess of probe molecules. The IR spectroscopy were recorded in the range of 400–4000 cm⁻¹.

in situ electron spin resonance (*in situ* ESR) signals were recorded with a Bruker A300 spectrometer. 30 mg powder sample was pressed into a self-supporting *in situ* ESR quartz tube. Before the ESR measurement was initiated, the tube was treated under dynamic vacuum (2.7×10⁻³ Torr) to remove surface contaminants. The ESR spectra of the sample was recorded.

in situ CO-adsorbed FTIR spectra were obtained on a Nicolet 6700 diffuse reflectance infrared spectrometer equipped with a stainless steel *in situ* IR flow cell. Firstly, the sample was preheated in N₂ flow for 30 min at 150 °C. After cooling down to 130 °C, a reference spectrum was recorded. Secondly, CO was introduced in constant flow and then N₂ was introduced to sweep the gaseous CO, the spectra were recorded at resolution of 4 cm⁻¹.

Computational methods and models

The bulk structure of T-phase Nb₂O₅ were modelled based on the reported structure.¹ The T-Nb₂O₅ surface model was constructed from the calculated T-Nb₂O₅ bulk structure in the (001) direction, with a 1×2 supercell in the two lateral directions. The oxygen vacancy defected Nb₂O₅ surface model was built by removing four oxygen atoms from the surface (Fig. S1). During optimization, all atoms were allowed to relax except for the bottom one layer that was kept frozen (represented as stick model in Fig. S1b and Fig. S1d). The Pd₄ cluster was used to simulate the Pd particle. All the spin-polarized electronic structure calculations were performed using the plane-wave periodic density functional theory as implemented in the Vienna *ab initio* simulation package (VASP).²⁻⁴ The projector augmented-wave (PAW) method developed by Blöchl⁵ was employed to describe the electron–ion interactions using plane wave basis

sets. The generalized gradient approximation (GGA) with the Perdew-Burke-Ernzerh (PBE) exchange-correlation functional was used.⁶ The kinetic energy cutoff was set to 450 eV. The convergence criteria for the energy calculations were set to a self-consistent field (SCF) tolerance of 1.0×10^{-5} eV. All internal structure parameters were relaxed until the maximum Hellmann–Feynman force on each ion were less than 0.02 eV/Å. Integration over the Brillouin zone was achieved with k-points mesh of $9 \times 5 \times 9$ for T-phase Nb₂O₅ bulk model optimization and $2 \times 1 \times 1$ for surface model optimization according to the Monkhorst-Pak scheme⁷ together with a Gaussian smearing broadening of 0.05 eV. The numerical calculation of the second derivatives of the harmonic potential energy surface provided the vibrational frequencies and corresponding normal modes. A geometrical displacement of 0.01 Å was used for all vibrational calculations. The final electronic energies were calculated using RPBE functional⁸ based on the optimized geometries.

Table S1. Catalytic performance of Pd/Nb₂O₅ catalysts with different Pd content.

Catalysts	Designed Pd content (%)	Measured Pd content (%)	CO conversion (%)	DMO selectivity (%)	WTY of DMO (g·kg _{cat.} ⁻¹ ·h ⁻¹)
Cat-1	0.1	0.098	28.2	82.3	513.9
Cat-2	0.3	0.295	37.8	86.4	723.1
Cat-3	0.5	0.497	43.4	88.2	847.6
Cat-4	1.0	0.992	63.1	92.9	1297.9
Cat-5	2.0	1.989	54.6	89.1	1077.2

Reaction conditions: 0.2 g catalyst, 130 °C, 0.1 MPa, WHSV = 3000 L·kg_{cat.}⁻¹·h⁻¹, CO: MN: Ar: N₂ = 28% : 18% : 4% : 50%.

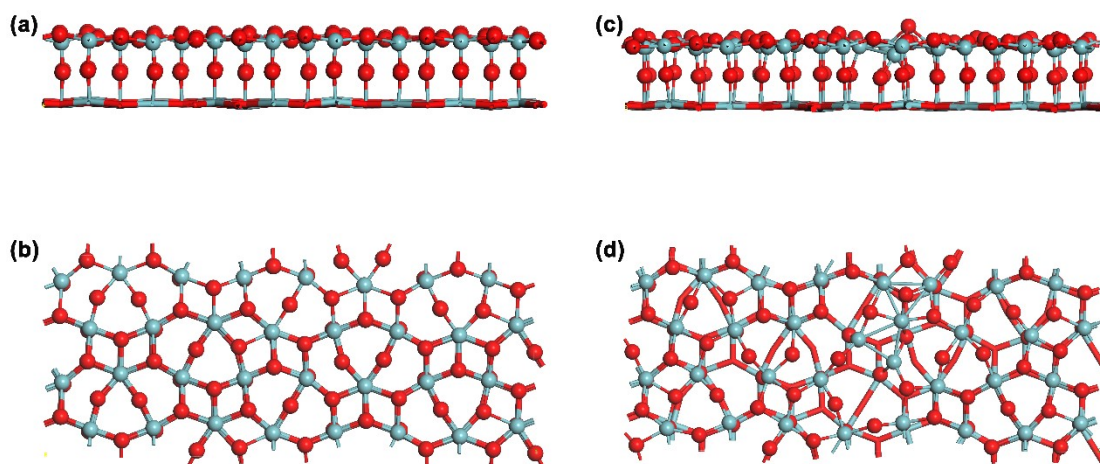


Fig. S1. (a) Front view and (b) top view for ideal Nb_2O_5 (001) surface, as well as the (c) front view and (d) top view for oxygen vacancy defected Nb_2O_5 (001) surface. The bottom one layer that is represented as stick model was kept frozen during geometry optimization.

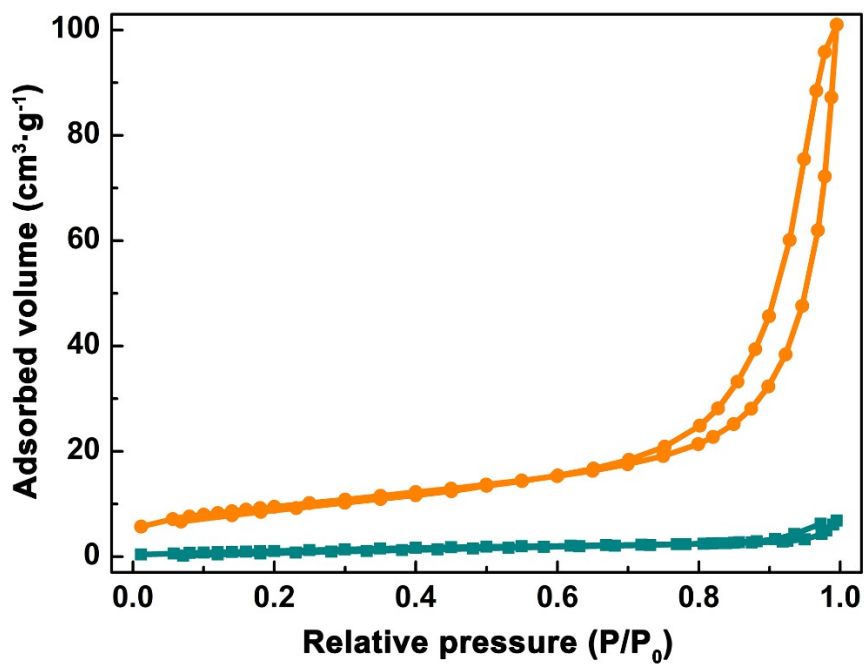


Fig. S2. N_2 adsorption-desorption isotherms at the temperature of 77 K for H- Nb_2O_5 (orange) and C- Nb_2O_5 (green) support.

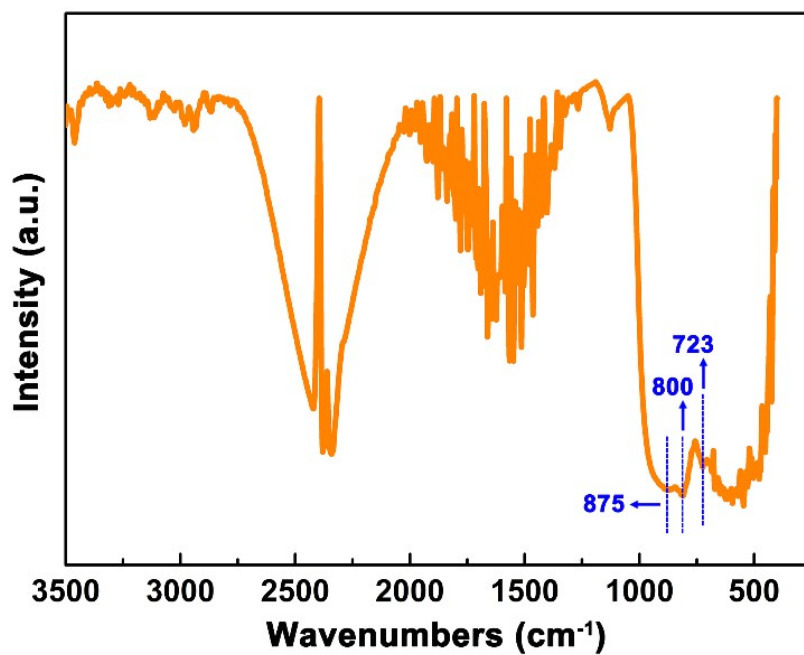


Fig. S3. FTIR spectra of H-Nb₂O₅ support.

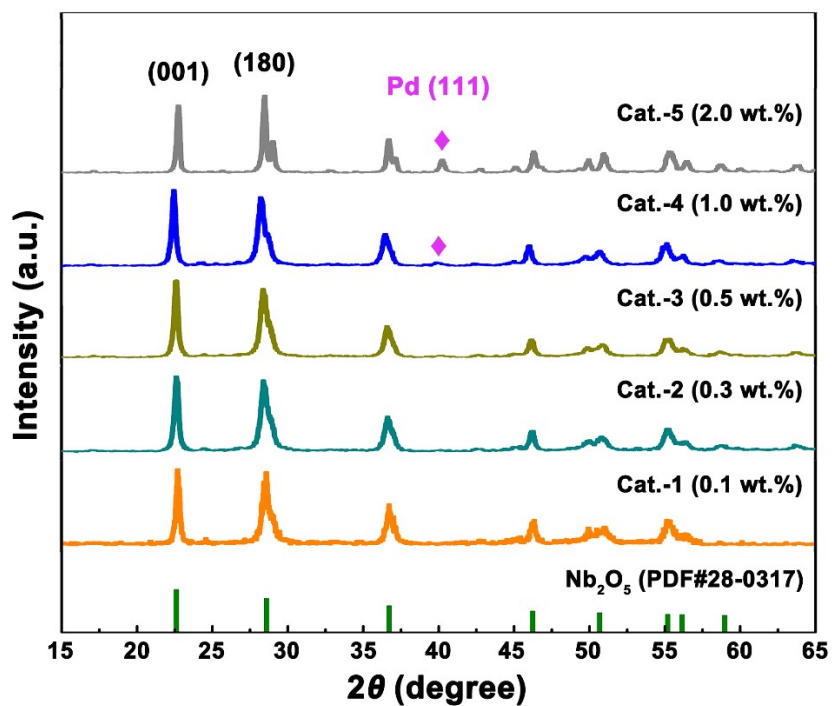


Fig. S4. PXRD patterns of Pd/H-Nb₂O₅ catalysts with different Pd content.

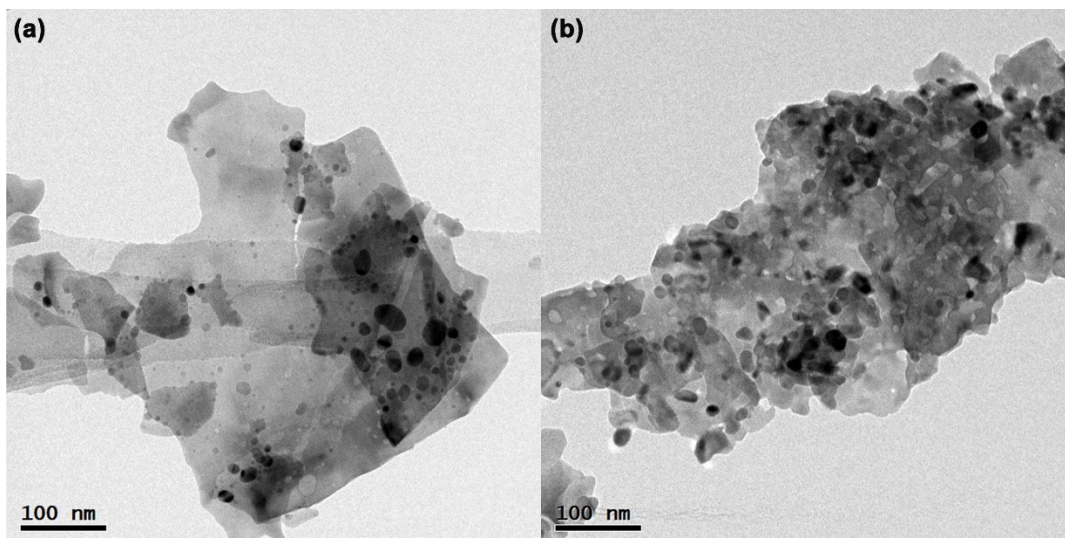


Fig. S5. TEM images of Pd/C-Nb₂O₅ catalyst with 1.0 wt.% of Pd content.

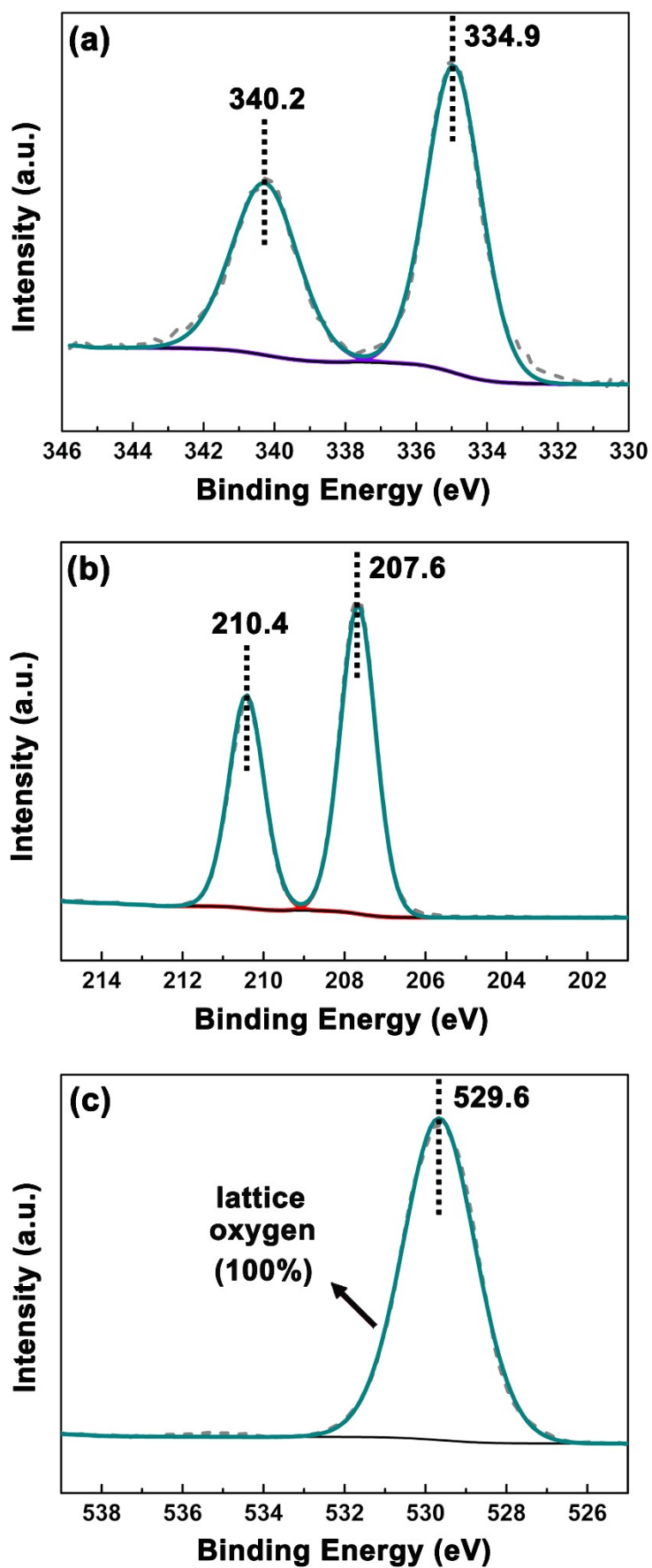


Fig. S6. (a) Pd 3d (b) Nb 3d (c) O 1s XPS of Pd/C-Nb₂O₅ catalyst.

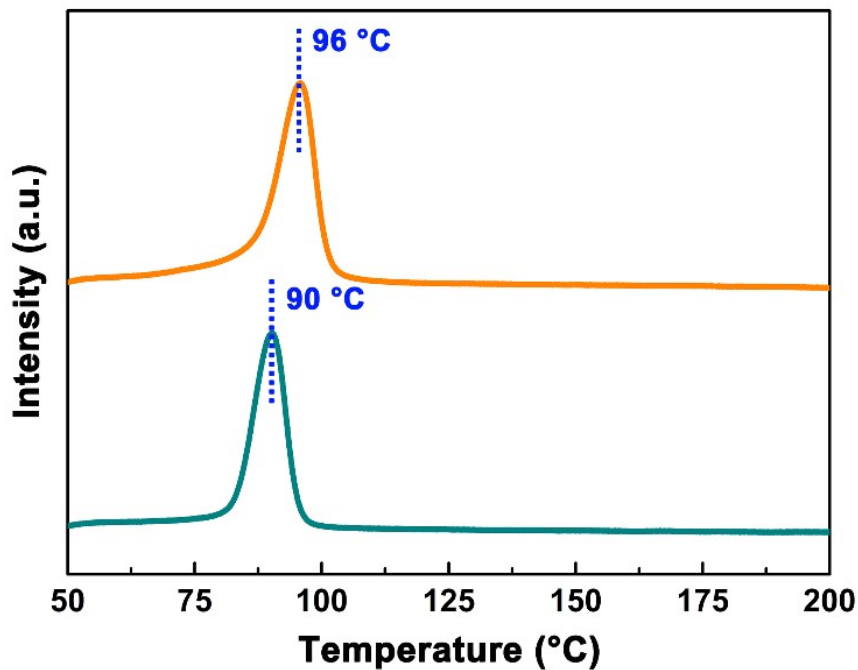


Fig. S7. H₂-TPR of air calcined Pd/H-Nb₂O₅ (orange) and Pd/C-Nb₂O₅ (green) catalyst.

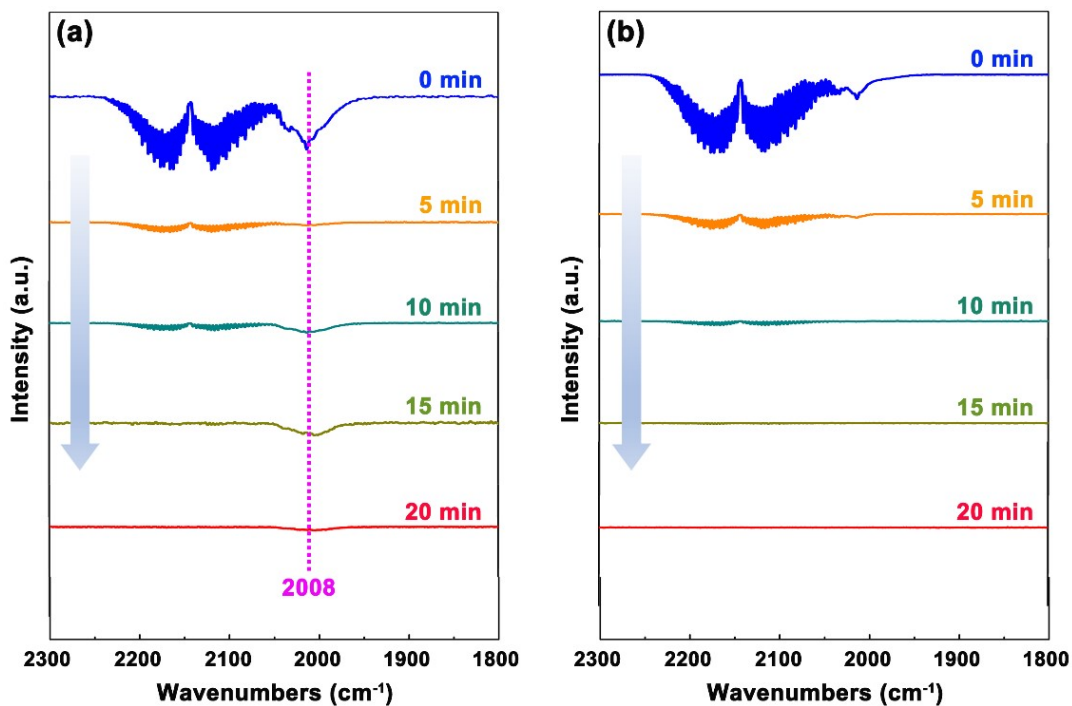


Fig. S8. *in situ* CO-adsorbed FTIR spectra of (a) pure H-Nb₂O₅ and (b) pure C-Nb₂O₅ support.

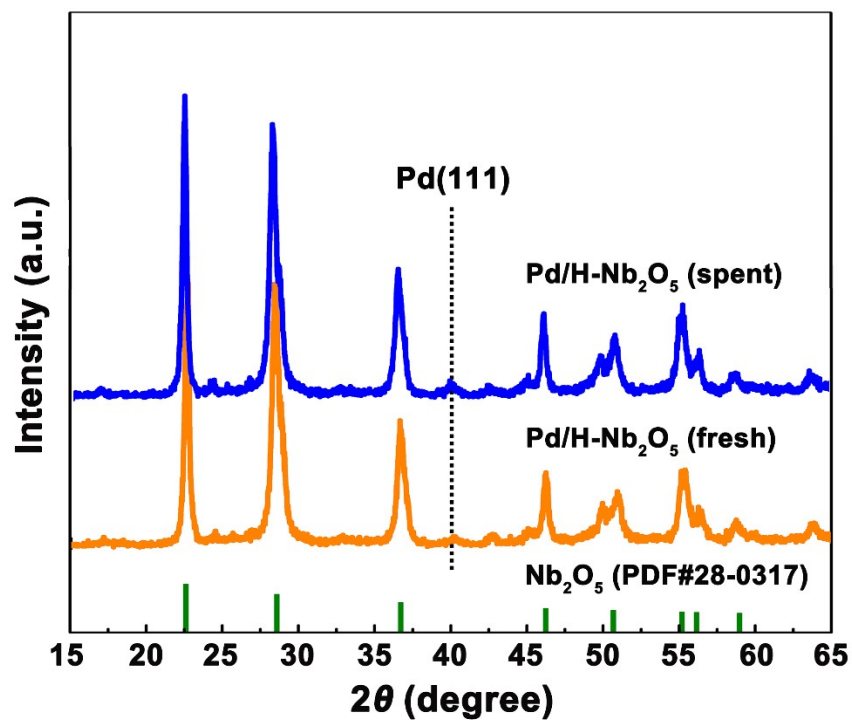


Fig. S9. PXRD patterns of fresh (orange) and spent (blue) Pd/H-Nb₂O₅ catalysts.

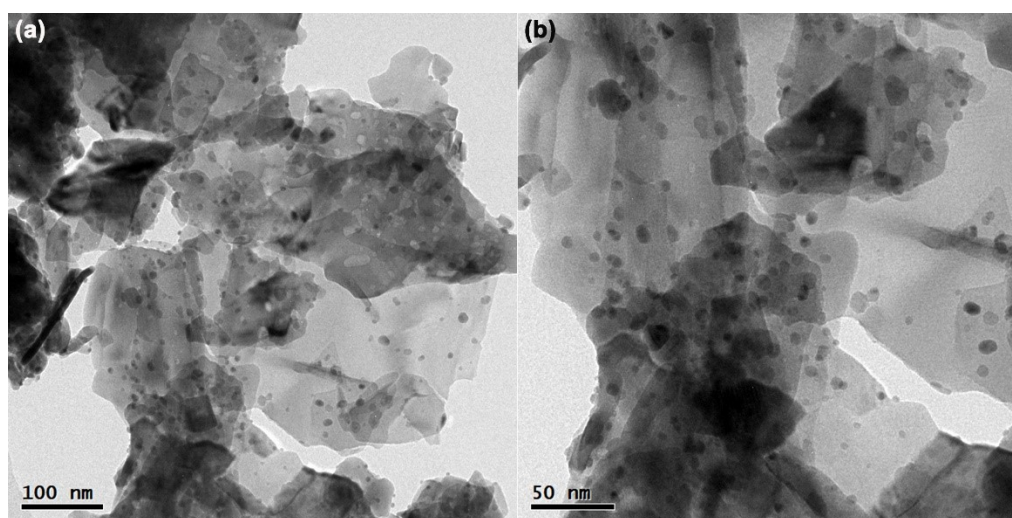


Fig. S10. TEM images of spent Pd/H-Nb₂O₅ catalysts.

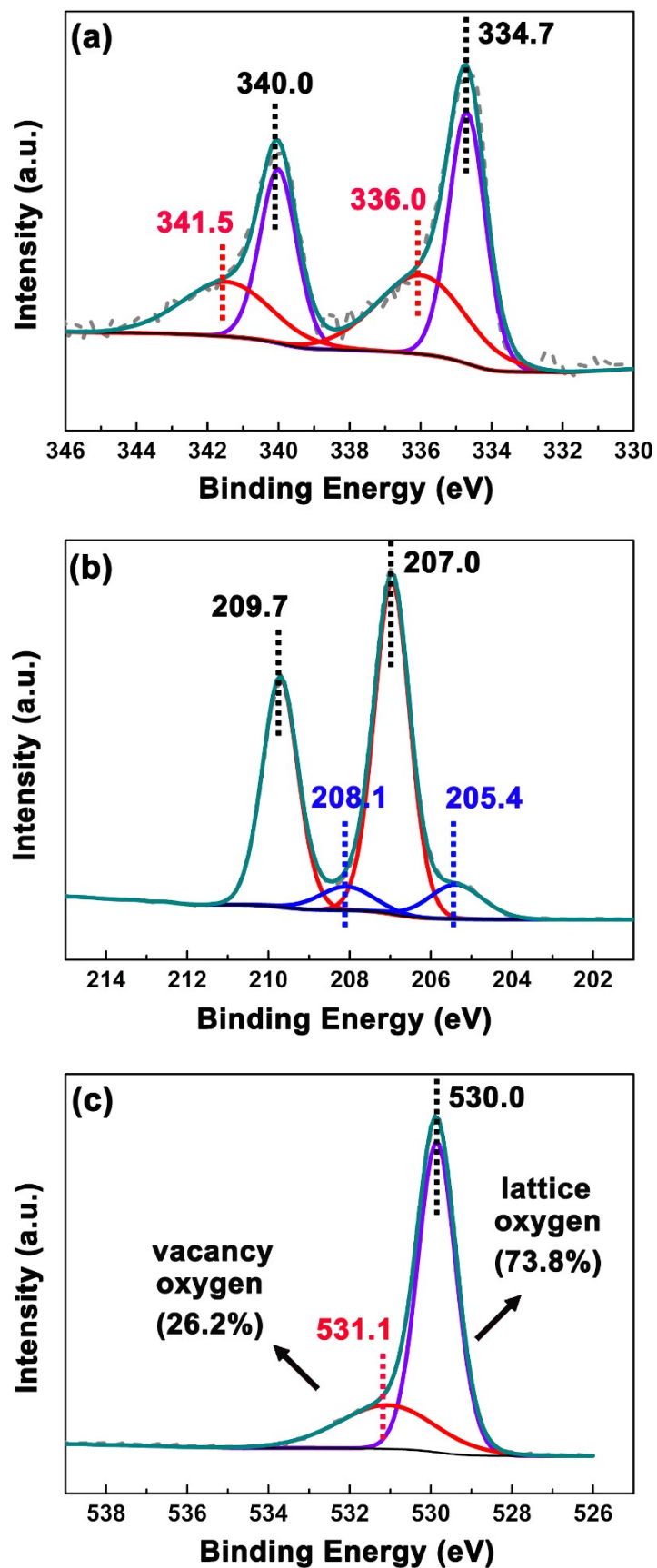


Fig. S11. (a) Pd 3d (b) Nb 3d (c) O 1s XPS of spent Pd/H-Nb₂O₅ catalyst.

References

1. Kato, K.; Tamura, S. Die kristallstruktur von T-Nb₂O₅. *Acta Crystallogr., Sect. B: Struct. Sci.* **1975**, *31*, 673-677.
2. Kresse, G.; Hafner, J. ab-initio molecular-dynamics for open-shell transition-metals. *Phys. Rev. B* **1993**, *48*, 13115-13118.
3. Kresse, G.; Furthmuller, J. Efficient iterative schemes for ab initio total-energy calculations using a plane-wave basis set. *Phys. Rev. B* **1996**, *54*, 11169-11186.
4. Kresse, G.; Furthmuller, J. Efficiency of ab-initio total energy calculations for metals and semiconductors using a plane-wave basis set. *Comput. Mater. Sci.* **1996**, *6*, 15-50.
5. Blochl, P. E. Projector Augmented-wave Method. *Phys. Rev. B* **1994**, *50*, 17953-17979.
6. Perdew, J. P.; Burke, K.; Ernzerhof, M. Generalized gradient approximation made simple. *Phys. Rev. Lett.* **1996**, *77*, 3865-3868.
7. Monkhorst, H. J.; Pack, J. D. Special points for Brillouin-zone integrations. *Phys. Rev. B* **1976**, *13*, 5188-5192.
8. Hammer, B.; Hansen, L. B.; Norskov, J. K. Improved adsorption energetics within density-functional theory using revised Perdew-Burke-Ernzerhof functionals. *Phys. Rev. B* **1999**, *59*, 7413-7421.